MATERIALS FOR ROBOTICS

Electrically programmable adhesive hydrogels for climbing robots

Junwen Huang[1,2], Yu Liu[3], Yuxin Yang[1], Zhijun Zhou[3], Jie Mao[1,2], Tong Wu[1], Jun Liu[1], Qipeng Cai[1], Chaohua Peng[1], Yiting Xu[1,2], Birong Zeng[1,2], Weiang Luo[1,2], Guorong Chen[1,2], Conghui Yuan[1,2]*, Lizong Dai[1,2]*

Although there have been notable advances in adhesive materials, the ability to program attaching and detaching behavior in these materials remains a challenge. Here, we report a borate ester polymer hydrogel that can rapidly switch between adhesive and nonadhesive states in response to a mild electrical stimulus (voltages between 3.0 and 4.5 V). This behavior is achieved by controlling the exposure and shielding of the catechol group through water electrolysis–induced reversible cleavage and reformation of the borate ester moiety. By switching the electric field direction, the hydrogel can repeatedly attach to and detach from various surfaces with a response time as low as 1 s. This programmable attaching/detaching strategy provides an alternative approach for robot climbing. The hydrogel is simply pasted onto the moving parts of climbing robots without complicated engineering and morphological designs. Using our hydrogel as feet and wheels, the tethered walking robots and wheeled robots can climb on both vertical and inverted conductive substrates (i.e., moving upside down) such as stainless steel and copper. Our study establishes an effective route for the design of smart polymer adhesives that are applicable in intelligent devices and an electrochemical strategy to regulate the adhesion.

INTRODUCTION

Climbing robots have been of great interest for fundamental research and for industry or military applications (*1*–*3*). A key challenge for the field of climbing robots is to realize programmable surface attachment/detachment. Over the past decades, scientists have attempted to address this issue mainly from the morphological design of materials or engineering control over robot motion systems. A representative example of the morphological strategy involves a biomimetic approach inspired by geckos, which is normally based on the microstructure materials design (*4*–*9*). Recent advances in improving the locomotion performance of biomimetic climbing robots mainly focus on the integration of both gecko-inspired microstructure and material's inherent adhesive property (*10*, *11*). The attaching/detaching behavior of these biomimetic robots is programmed through adjusting the interaction direction between the robot feet and the substrates or controlling the mechanical property of the foot materials. Other strategies for climbing robots—including electrostatic adsorption (*12*), magnetic interaction (*13*), and vacuum adsorption (*14*)—are based on well-developed engineering routes, which rely on the advance of motion control systems. In addition, these strategies often need external assistance such as a high voltage (≥1000 V) generator, a magnetizable substrate, or a predesigned surface.

Intrinsically adhesive materials (IAMs), with their intrinsic adhesive property derived from van der Waals interaction (*9*), hydrogen bonding (*15*), ligand coordination (*16*), or host-guest interaction (*17*), have potential applications in the design of motion systems for climbing robots. Benefiting from the control over materials composition and microstructure, IAMs with enhanced adhesion strength (*18*–*21*), excellent stability (*22*, *23*), and wet surface or underwater adaptability (*24*, *25*) have been developed. It is also possible for IAMs to change their adhesiveness in response to stimuli like pH (*26*, *27*), pressure (*28*), water (*29*), temperature (*30*, *31*), etc. Particularly, mussel-inspired IAMs using catechol groups as adhesive promoters have been widely exploited for dry, wet, and underwater adhesion (*32*, *33*). Catechol groups can bind to various surfaces via interactions such as ligand coordination, hydrogen bonding, and electrostatic adsorption (*34*). Because of the excellent adhesive properties, catechol-based IAMs show promising applications in the fields of sensing (*35*), biomedicine (*36*), energy (*37*), and surface engineering (*38*).

However, there have been few examples demonstrating the practical use of IAMs in climbing robots for several reasons. First, a small subset of IAMs can reversibly and rapidly switch between adhesive and nonadhesive states. Second, the abovementioned adhesion evolution triggers are impractical for climbing robots. For example, it is hard to precisely control the pH, temperature, and water content of IAMs or the environment during robot climbing. Third, many IAMs exhibit stimuli-responsive adhesion to limited or predesigned substrates. We envisaged that a rationally designed catechol-based IAM that exposes and shields its catechol groups on demand could enable programmable adhesion. Moreover, we expected to trigger the adhesion evolution of IAMs using an electrical stimulus, because the intensity, frequency, and switch of an electric field can be readily programmed. To demonstrate this concept, we designed a hydrogel-type IAM through a borate ester formation reaction involving boric acid (BA), catechol, and poly(vinyl alcohol) (PVA). This design was based on the fact that inorganic BA and organic boronic acids have a high condensation reaction activity with 1,2-diol or 1,3-diol functionalized molecules or polymers (*39*, *40*). The as-formed borate esters or boronate esters are cleavable in response to acidic pH or guest molecules (*41*). We anticipate that water electrolysis at the interface between the hydrogel and the conductive substrate can change the pH and cause the reversible

[1]College of Materials, Xiamen University, Xiamen 361005, People's Republic of China. [2]Fujian Provincial Key Laboratory of Fire Retardant Materials, Xiamen University, Xiamen 361005, People's Republic of China. [3]School of Aerospace Engineering, Xiamen University, Xiamen 361005, People's Republic of China.
*Corresponding author. Email: yuanch@xmu.edu.cn (C.Y.); lzdai@xmu.edu.cn (L.D.)

cleavage/reformation of borate ester moiety, thus controlling the exposing/shielding of catechol groups. Our hydrogels not only showed characteristics of rapid self-healing, high stretchability, and ionic conductivity but also exhibited programmable surface attachment/detachment in response to an electrical stimulus (voltages between 3.0 and 4.5 V). By introducing this electrically responsive hydrogel into both walking and wheeled robots, we demonstrated an alternative strategy for the climbing of robots on vertical and inverted surfaces.

RESULTS

Physical and mechanical properties

The hydrogel synthesis is straightforward and scalable. As illustrated in Fig. 1A, starting from commercial resources of 5,5′,6,6′-tetrahydroxy-3,3,3′,3′-tetramethyl-1,1′-spirobiindane (TTS) and BA, an oligomer cross-linker (denoted as TB) terminated with two tetrahydroxyborate anions was synthesized in a KOH solution. Then, the cross-linking reaction between TB and PVA led to the formation of borate ester hydrogels (denoted as TBVA). The pH of the hydrogels was controlled at ~8.5, because a weak alkalinity condition could ensure the integrity of cross-linked polymer networks and the rapid electrical response. Because we intended to apply this hydrogel in climbing robots, we optimized its mechanical performances through the cross-linking density control. By changing the TB content from 1.0, 2.0, 4.0, to 6.0 weight % (wt %), we prepared four TBVA hydrogel samples named TBVA1, TBVA2, TBVA3, and TBVA4, respectively. The water content of TBVA1 to TBVA4 was fixed at ~85 wt % because this water content was beneficial to both mechanical and adhesive properties. The composition and structure of TB and TBVA hydrogels were characterized. Briefly, in the Fourier transform infrared (FTIR) spectrum of TB, the detection of an absorption band at 1398 cm^{-1}, characteristic of the B—O—C stretching of borate ester (*42*), confirms the condensation reaction between TTS and BA (fig. S1 and table S1). The ^{1}H nuclear magnetic resonance (NMR) spectrum (fig. S2) indicates that TB is an oligomer with an average polymerization degree of ~3. The characteristic peaks of both TB and PVA emerge in the FTIR spectrum of TBVA hydrogels (fig. S3A). Specifically, the B—O—C stretching signal of borate ester shifts to lower wave numbers (1385 cm^{-1}), because some of the borate esters are formed between TB and PVA (*43*, *44*). X-ray photoelectron spectroscopy (XPS) results (fig. S3B) further verify the presence of borate ester and conductive borate salts in TBVA hydrogels.

TBVA hydrogels were processed into square pieces with a flat surface using poly(tetrafluoroethylene) (PTFE) molds. The as-obtained hydrogel samples display a nontransparent appearance (Fig. 1B) and hydrophobic surfaces (Fig. 1C). The contact angles of water on the hydrogel surfaces are 134.0° ± 2° (TBVA1), 139.4° ± 3° (TBVA2), 131.9° ± 2° (TBVA3), and 121.2° ± 3° (TBVA4). A control sample prepared by cross-linking PVA only with BA (denoted as BVA hydrogel) shows a water contact angle of 18.9 ± 3° (fig. S4A), demonstrating a hydrophilic characteristic. These results imply that the

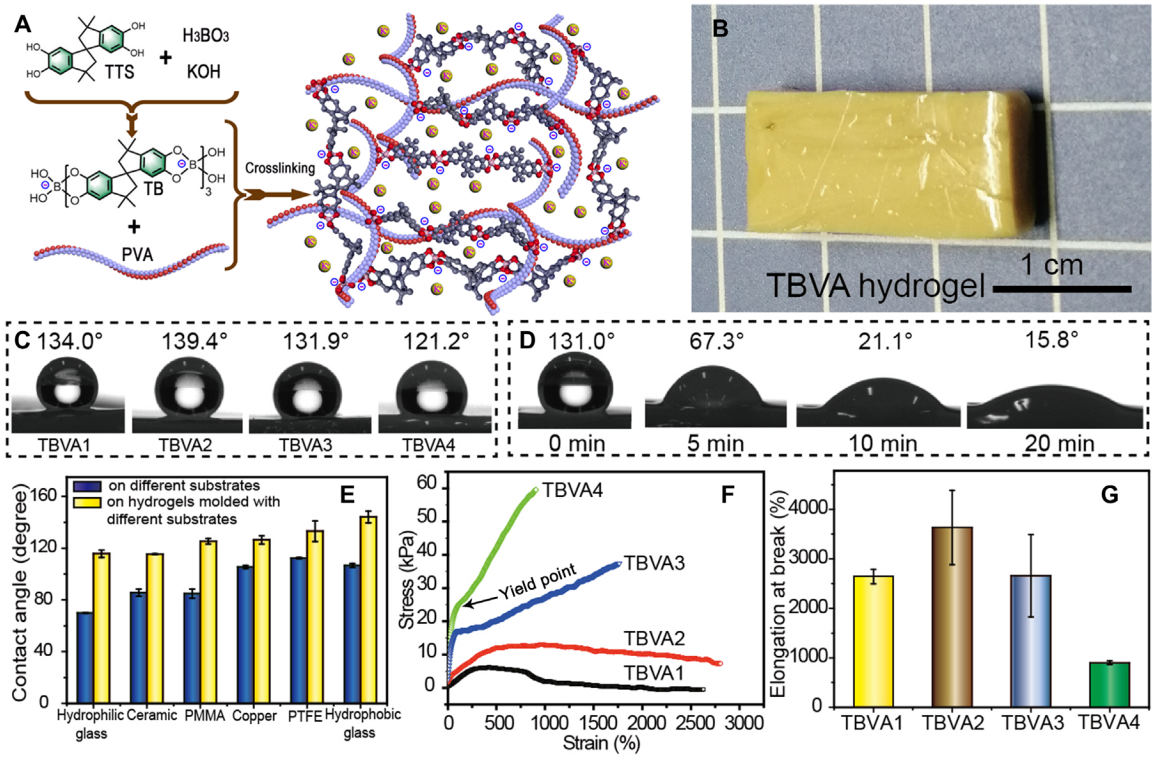

Fig. 1. Surface and mechanical properties of TBVA hydrogels. (**A**) Synthetic procedure and molecular structure of TBVA hydrogels. (**B**) Photograph of a typical TBVA hydrogel. (**C**) Photographs of water droplets on the hydrogels shaped with a PTFE mold. (**D**) Contact angle evolution of a water droplet on TBVA3 over time. (**E**) Water contact angles on TBVA3 molded by different substrates. Tensile stress-strain curves (**F**) and elongations at break (**G**) of the hydrogels. TBVA is the abbreviation of the borate ester polymer hydrogels, whereas TBVA3 is the hydrogel sample prepared by using 4.0 wt % of cross-linker. Error bars represent the SD for $n = 5$ measurements at each data point.

hydrophobic moiety (derived from TB) can shield the hydrophilic components (including PVA chains and tetrahydroxyborate anions) in the polymer networks. The hydrophilic components in TBVA hydrogels can migrate to the surface in response to a change of interface environment. For example, the contact angle of a water droplet on the surface of TBVA3 decreases from 131.0° to 15.8° (Fig. 1D) with the prolonging of contacting time from 0 to 20 min. The same phenomenon was observed when molding TBVA hydrogels with different substrates. Shaping the hydrogels with hydrophobic molds can maintain or even improve the surface hydrophobicity, whereas molding the hydrogels with hydrophilic substrates can reduce the surface hydrophobicity (Fig. 1E and fig. S4B).

From the tensile tests, TBVA1, TBVA2, TBVA3, and TBVA4 have yield strengths of ~1.2, ~4.2, ~16.8, and ~22.5 kPa and maximum strengths of ~6.1, ~12.7, ~38.1, and ~60.1 kPa, respectively (Fig. 1F and table S2). All samples show high stretchability (Fig. 1G). The elongations at break of the hydrogels are ~2641% (TBVA1), ~3635% (TBVA2), ~2656% (TBVA3), and ~913% (TBVA4). Apparently, increasing the cross-linking density of TBVA hydrogels can improve the mechanical strength but reduce the stretchability. The water content of TBVA hydrogels affects their mechanical properties. For example, TBVA3 with 90 wt % water content only has a yield strength of ~4.3 kPa, whereas TBVA3 with reduced water content (80 wt %) maintains a high yield strength of ~17.2 kPa (fig. S5). The rheological properties of the hydrogels were tested. Hydrogels with a large storage modulus (G') normally have stable cross-linked polymer networks. In contrast, a high loss modulus (G'') implies that the polymer chains have excellent mobility, and the hydrogels exhibit viscous behavior. As illustrated in fig. S6, TBVA1 with the lowest cross-linking density mainly exhibits viscous behavior, whereas TBVA2 to TBVA4 display both elastic and viscous behaviors. The order of G' value is TBVA4 > TBVA3 > TBVA2 > TBVA1, which agrees well with the results of tensile test. For the strain (γ) sweeps of TBVA2 to TBVA4, G' and G'' start to decrease at $\gamma > 30\%$, implying that these hydrogels can keep an intact structure at $\gamma \leq 30\%$. The dynamical feature of the hydrogel polymer networks can be confirmed by the frequency (ω) sweep, because the gaps between G' and G'' of all samples become larger with the increasing of ω (*45*, *46*). The temperature (T) sweep is usually applied to track the sol-gel transformation of the hydrogels. During the temperature sweep, $G' > G''$ indicates a gel state, and $G' < G''$ implies a sol state. Accordingly, TBVA1 is in a sol state at $25°C \leq T \leq 80°C$, whereas TBVA2 to TBVA4 maintain a good gel state at $25°C \leq T \leq 42°C$. These results suggest that TBVA2 to TBVA4 have promising mechanical performances at room temperature and under small strains.

TBVA hydrogels also have rapid self-healing capability. Figure 2A and movie S1 visually illustrate the self-healing process of TBVA3. After connecting four pieces of TBVA3 together for 2 min, the self-healed hydrogel can bear 100 g of weight. Optical microscopy images (Fig. 2B and fig. S7A) indicate that cracks with ~30 μm of width can be repaired completely within 5 min. By combining two pieces of TBVA3 together for 1 min, the reformed hydrogel can be stretched 400% (Fig. 2C). With a healing time longer than 0.5 min, all self-healed hydrogels demonstrate a tensile behavior similar to their corresponding original hydrogels (Fig. 2D). In consideration of the maximum strength, the self-healing efficiency of TBVA3 reaches 79, 91, and 99% within 0.5, 1, and 2 min (Fig. 2E), respectively. In the case of control sample BVA, the self-healing efficiency within 2 min is only 45.2% (fig. S7B). Continuous step strain sweep of rheological measurement further indicates the self-healing characteristic of TBVA hydrogels. As shown in Fig. 2F, G' and G'' of TBVA3 reduce by ~95.3 and ~79.1% at $\gamma = 80\%$, respectively, but easily recover within 2 min at $\gamma = 0.5\%$. This result indicates that the hydrogels recover their polymer networks rapidly. The self-healing performance was also confirmed by the conductivity measurement. From the Nyquist impedance plots (fig. S8A), the conductivities of TBVA1, TBVA2, TBVA3, and TBVA4 are ~1.62, ~2.31, ~4.29, and ~4.00 mS/cm, respectively, implying that the conductivity of TBVA hydrogels is only at the medium level in terms of hydrogel-type electrolytes (*47*). In TBVA hydrogels, the dominant conductive ions are K^+ and OH^-. Besides, $K_2B_4O_7$ (as evidenced by the XPS result in fig. S3B) and tetrahydroxyborate anions may contribute to the hydrogel conductivity (*48*, *49*). Because most of these ions are introduced into TBVA hydrogels by the cross-linker TB, it is understandable that a higher content of cross-linker leads to an improved conductivity. However, excessively cross-linked polymer networks can hinder the ion transfer (*50*). Thus, TBVA3 with a moderate

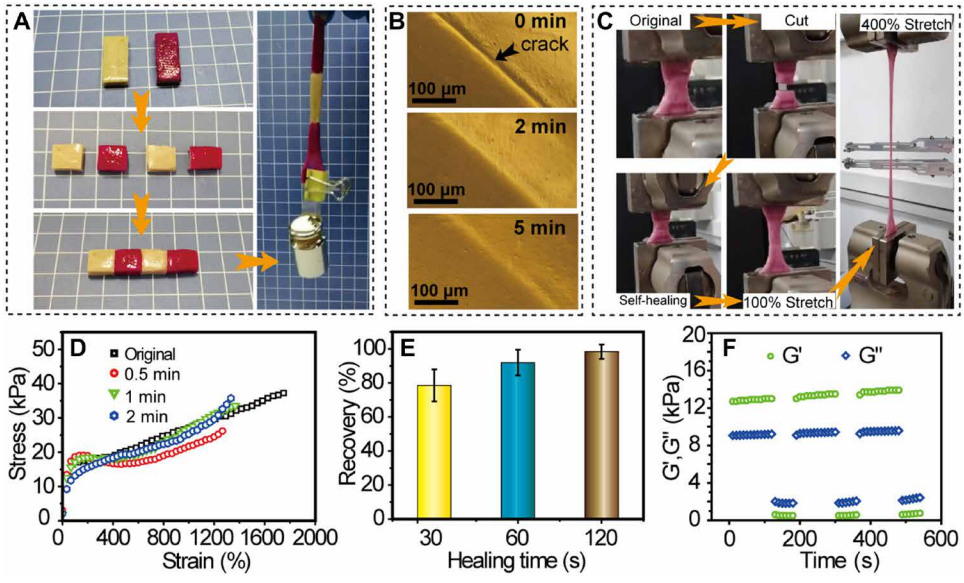

Fig. 2. Self-healing performances of TBVA hydrogels. (**A**) Photographs illustrating the self-healing behavior of TBVA3; the weight is 100 g, and the sample size is 0.4 cm by 0.1 cm by 3.0 cm. (**B**) Optical micrographs tracking the crack recovery on the surface of TBVA3 under ambient conditions. (**C**) Tensile behavior of self-healed TBVA3; the experiment procedure was set as follows: original TBVA3 → cut → 1 min of self-healing → 100% stretch → 400% stretch. (**D**) Tensile stress-strain curves of original and self-healed TBVA3. (**E**) Tensile strength recovery efficiency of self-healed TBVA3. (**F**) Time dependences of storage modulus (G') and loss modulus (G'') in continuous step strain measurements of TBVA3. Red samples in the pictures were colored with rhodamine B. Error bars represent the SD for $n = 5$ measurements at each data point.

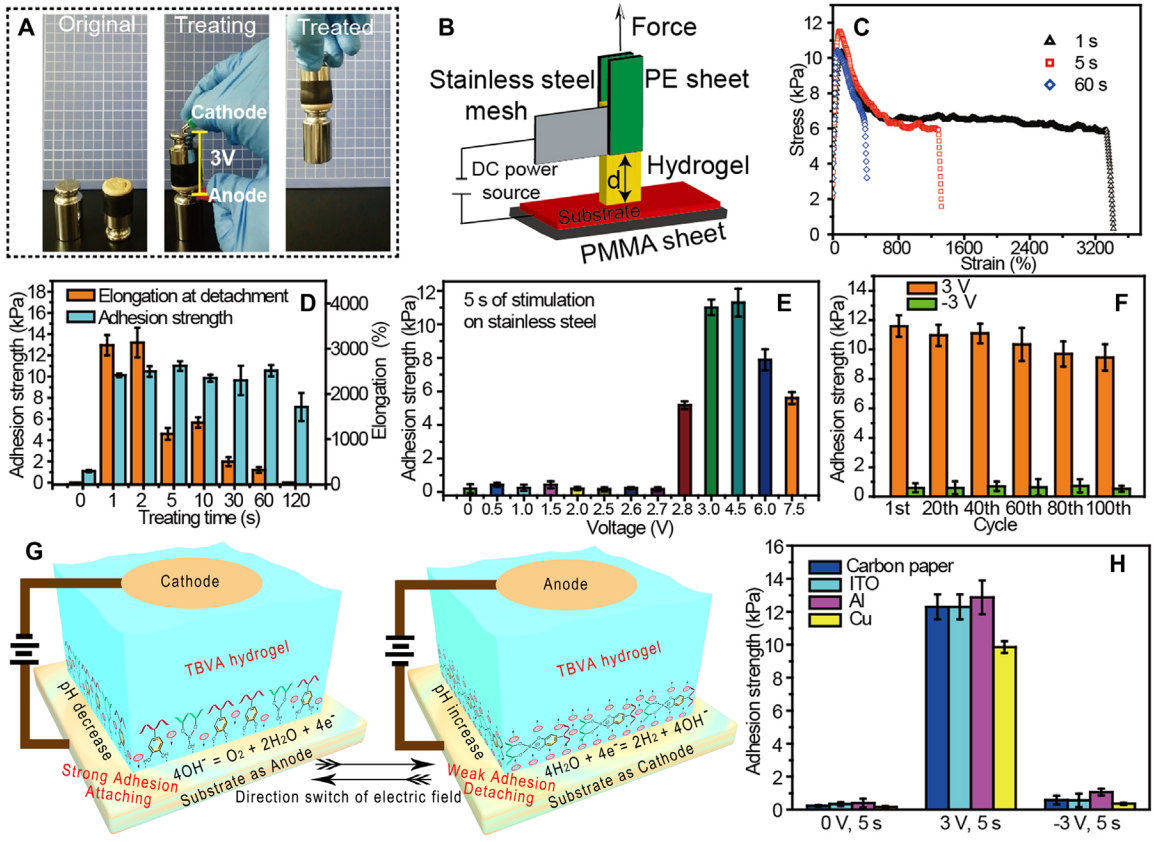

Fig. 3. Electrically programmable adhesion of TBVA hydrogels. (**A**) The adhesiveness of TBVA3 triggered by an electrical stimulus (voltage, 3.0 V; stimulation time, 4 s) can carry 100 g of weight (surface area, 3.14 cm^2). (**B**) Schematic illustration for adhesion test device. The gap between two electrodes (*d*) is 1.5 cm. (**C**) Tensile stress-strain curves of TBVA3 attached to stainless steel under different electrical stimulation times (voltage, 3.0 V). (**D**) Effect of electrical stimulation time on the adhesion strength and elongation at detachment of TBVA3 on stainless steel (voltage, 3.0 V). (**E**) Adhesion strength evolution of TBVA3 on stainless steel versus voltage (stimulation time, 5 s). (**F**) Adhesion strength evolution of TBVA3 when switching the electric field direction (voltage, 3.0 V; 2 s for attachment and 3 s for detachment). (**G**) Proposed mechanism for the electrically programmable adhesion of TBVA hydrogels. (**H**) Adhesive/nonadhesive evolution of TBVA3 on different surfaces; experiment procedure: 0 V, 5 s for contact → 3.0 V, 5 s for attachment → −3.0 V, 5 s for detachment. Error bars represent the SD for $n = 5$ measurements at each data point.

cross-linking density exhibits the best conductivity. After combining two pieces of hydrogels together, the reformed hydrogel recovers its conductivity efficiently (fig. S8B). The self-healing ability of TBVA hydrogels is attributed to the presence of dynamic borate ester cross-linking sites, which can be cleaved and reformed under ambient conditions (*39*, *51*, *52*). Also, the high mobility of functional groups and polymer chains in TBVA hydrogels can accelerate the self-healing process.

Electrically programmable adhesion

Under ambient conditions, TBVA hydrogels are not particularly adhesive to any substrate. However, their adhesiveness can be activated by electrical stimulation. After comprehensively considering the hydrogel mechanical and conductive properties, we chose TBVA3 as an example for the adhesion test. As visually displayed in movies S2 and S3 and Fig. 3A, when a piece of TBVA3 is sandwiched between two stainless steel electrodes, the adhesion is generated only at the anode. A device schematically illustrated in Fig. 3B was designed to track the adhesion strength evolution (movie S4). Typical tensile stress-strain curves of TBVA3 attached to stainless steel are given in Fig. 3C. The adhesion strengths and elongations at detachment are shown in Fig. 3D. Without an electrical stimulus, the adhesion strength is only ~0.5 kPa, indicating a weak interaction. Under a 3.0-V electric field, 1 s of stimulation results in ~10.2 kPa of adhesion strength. Within 5 s, TBVA3 reaches the largest adhesion strength of ~11.5 kPa. Further prolonging the stimulation time declines the adhesion strength. From the elongation results, 2 s of stimulation leads to the largest elongation at detachment (3200%), which is close to the tensile test result of TVBA3 itself.

To attach TBVA hydrogels to stainless steel, the promising voltage region is 3.0 to 4.5 V, as the adhesion strength reaches optimized values within 5 s (Fig. 3E). When setting the voltages to 2.7 and 2.5 V, TBVA3 requires 30 and 300 s to generate ~8.5 and ~7.6 kPa of adhesion strengths, respectively (fig. S9). Electrical stimuli with voltages lower than ~2.4 V cannot cause the adhesiveness of TBVA hydrogels. A high voltage is not helpful for adhesion generation. For example, a voltage of 6.0 V (5 s) only induces ~7.8 kPa of adhesion strength. When increasing the gap between two electrodes from 1.5 to 2.0 cm, 60 s of electrical stimulation (3.0 V) is needed for the hydrogel to reach the optimized adhesion strength (fig. S10). We also tested the influence of water content on the adhesive performance of the hydrogels. As shown in fig. S11, TBVA3 with reduced water content (80 wt %)

generates ~10.8 kPa of adhesion strength after 5 s of electrical stimulation (3.0 V). Under the same condition, TBVA3 with a higher water content (90 wt %) only shows adhesion strength of ~2.2 kPa.

The adhesion of TBVA hydrogels to stainless steel can be rapidly switched by simply changing the electric field direction. After applying a negative electric field (−3.0 V), the hydrogels detach from stainless steel (cathode) (movies S2 and S5). By programming the electric field direction, TBVA hydrogels can reversibly attach to and detach from stainless steel. We also tracked the adhesion strength evolution of TBVA3 during cycling. The stimulation mode was set as follows: positive electric field (3.0 V, 2 s) and negative electric field (−3.0 V, 3 s). With the cycling of the electric field, the adhesiveness of TBVA3 hydrogel can be repeatedly switched (Fig. 3F). After 100 cycles, TBVA3 shows ~12.7% decline in adhesion strength, demonstrating its relatively high cyclability.

Recently, Lee's group (*26*, *27*, *53*) made progress in understanding the adhesion evolution of catechol-based IAMs. They found that the pH increase of catechol-functionalized polymer solutions induced by water electrolysis promoted catechol oxidation, thus deactivating the adhesiveness. Also, they explained the relevance between pH and adhesion of catechol-boronate polymers from the perspective of dynamic boronate ester. These contributions enlightened us to find the underlying mechanism for the electrically programmable adhesion of TBVA hydrogels, through both electrochemical process and surface composition evolution. We first characterized the cyclic voltammetry (CV) curves of TTS and TB using a three-electrode system (potential window, −0.5 to 0.5 V). TTS exhibits a typical redox activity with oxidation and reduction potentials of ~0.01 and ~−0.13 V (versus Hg/HgO), respectively (fig. S12A). However, TB does not have this redox behavior in the electrochemical systems with either glassy carbon or stainless steel as the working electrode (fig. S12, A and B). It is likely that concealing the catechol group in the borate ester can improve its electrochemical stability. In the three-electrode system with a stainless steel electrode, we also tested the CV curves of TB using an extended potential window of −3.0 to 3.0 V. In this case, notable water electrolysis occurred, as evidenced by the bubble release from the stainless steel electrode (movie S6). The corresponding CV curve (fig. S13A) shows that the onset potentials of oxygen evolution reaction (OER) and hydrogen evolution reaction (HER) are ~1.32 and ~−1.41 V (versus Hg/HgO), respectively. To more accurately track the electrochemical process during the adhesiveness variation, we sandwiched TBVA3 between two stainless steel electrodes and acquired the CV curve using a so-called two-electrode system (potential window, −3.0 to 3.0 V). Electrochemical signals in the as-obtained CV curve (fig. S13B) are similar to that of TB (fig. S13A). However, because these two CV curves were measured by using different modes, the signal potentials were different. The onset potentials of OER and HER of TBVA3 system are ~2.33 and ~−2.30 V, respectively. The redox reaction of catechol group cannot be observed to TBVA3 either.

The above electrochemical results reveal two key points relating to the electrically switchable adhesion of TBVA hydrogels: (i) this stimuli-responsive behavior is accompanied by a water electrolysis reaction, and (ii) the adhesiveness can only be activated at voltages higher than the onset potential of OER. Because TBVA hydrogels are alkaline, the water electrolysis reaction reduces the pH of the hydrogel surface contacting the anode but increases the pH at the cathode interface. Probably the adhesive activity of TBVA hydrogels is essentially controlled by pH. To verify this, we directly regulated the acidity and alkalinity of the hydrogel surface by submerging the hydrogel samples in aqueous solutions with different pH values (fig. S14) and tracked their adhesion evolution to stainless steel. As illustrated in fig. S15, the adhesiveness of TBVA hydrogels only emerges at a pH range of 2.0 to 6.0, and the largest adhesion strength appears at pH ~4.0.

We tracked the surface composition evolution of TBVA hydrogels during the electrical-response process (fig. S16). Because of the formation of borate ester, signals of the catechol group in the FTIR spectrum of TBVA hydrogels were not noticeable. After attaching to a stainless steel anode (3.0 V, 5 s), characteristic peaks of the catechol group at 1298 and 1508 cm^{-1} (C—O vibration of catechol and C═C vibration of aromatic ring) exhibited a prominent intensity increase. By switching the electric field direction, this hydrogel surface then contacted a stainless steel cathode (−3.0 V, 5 s). Evident attenuation in signal intensity of the catechol group occurred in the FTIR spectrum. As a control experiment, we conducted the water electrolysis reaction in TB solution using two stainless steel electrodes. Electrodeposition only appeared at the anode side (inset of fig. S17). FTIR spectrum of the deposited layer on the anode shows characteristic absorption peaks of TTS (fig. S17). In particular, signals of the catechol group are identifiable. On the basis of the composition analysis and electrochemical characterization, we confirm that the interface pH evolution caused by water electrolysis is the main driven force for the programmable adhesion of TBVA hydrogels. The molecular mechanism for this behavior is the reversible cleavage/reformation of borate ester, which controls the exposing/shielding of catechol group (Fig. 3G). Thus, the water electrolysis efficiency at the hydrogel/substrate interface determines the adhesion strength and response speed of TBVA hydrogels. According to this mechanism, it is understandable that (i) TBVA hydrogels cannot generate adhesiveness at voltages lower than the onset potential of OER; (ii) reducing the voltage or increasing the hydrogel thickness leads to a prolonged stimulation time to produce considerable adhesion strength; and (iii) a higher water content reduces the ion concentration and decreases the mechanical strength of the hydrogels, therefore weakening the electrically responsive performance. The weakened adhesiveness of TBVA hydrogels at a high voltage (such as 6.0 V) or a prolonged stimulation time (>5 s) is due to the excessive degradation of polymer networks under the strongly acidic condition (as evidenced by fig. S15). We also tracked the morphology and composition evolutions of the stainless steel surface during hydrogel attachment/detachment. As shown in fig. S18, under the stimulation mode of 2 s for attachment and 3 s for detachment (voltage, 3.0 V), stainless steel keeps an almost clean surface after 20 cycles of hydrogel attachment/detachment. However, when prolonging the electrical stimulation time (5 s for attachment and 5 s for detachment; voltage, 3.0 V, 20 cycles), a few hydrogel fragments emerge on the stainless steel surface. These results imply that the degraded TBVA hydrogels may adhere to the substrate surfaces, which is an important reason for the declined adhesion strength of the hydrogels after a long time cycling.

The programmable adhesion of TBVA hydrogels is adaptable to different situations. For example, they can be attached to different substrates under the same stimulating mode (fig. S19). Toward carbon paper, indium tin oxide (ITO) glass, aluminum (Al), and copper (Cu), TBVA3 generates adhesion strengths of ~12.6, ~12.2, ~12.9, and ~9.7 kPa, respectively, within 5 s of electrical stimulation (3.0 V). Upon applying a negative electric field (−3.0 V), TBVA3

detaches from these substrates within 5 s (Fig. 3H). We further evaluated the self-healing performance of TBVA hydrogels during attachment/detachment. As shown in fig. S20, surface-cracked TBVA3 exhibits no decay in adhesion strength to a stainless steel anode. Both response speed and cyclability of the surface-cracked hydrogel are comparable to that of the original hydrogel. During the attaching/detaching process, TBVA hydrogels can repair their surface cracks within 5 min.

Performances of climbing robots

Last, we demonstrate that TBVA hydrogels are applicable in climbing robots to achieve programmable locomotion on both vertical and inverted surfaces. We first designed a three-foot tethered walking robot (denoted as robot no. 1) for the climbing experiments (Fig. 4A). The weight of this robot is ~113 g (details for robot no. 1 can be found in Supplementary Text, table S3, and figs. S21 to S23). To each foot (foot A × 2 and foot B) of robot no. 1, we fixed a piece of TBVA hydrogel. The hydrogel sizes were about 6.0 cm by 1.8 cm by 0.4 cm for foot A and 7.5 cm by 2.7 cm by 0.4 cm for foot B. Carbon papers (thickness, 0.1 cm) were sandwiched between the hydrogels and the robot feet to act as current collectors. The circuit of each piece of hydrogel was independently controlled through a copper wire connecting the carbon paper to the power source. The voltage between the hydrogel and the substrate was switched between −3.0 and 3.0 V. A positive voltage meant that the electric current flowed from substrate to hydrogel; a negative voltage implied that the electric current flowed from hydrogel to substrate.

The climbing behavior of robot no. 1 was tested on both near-vertical (inclination, 85°) and inverted substrates. For a typical near-vertical locomotion cycle (Fig. 4B and movie S7), foot B first attached to the substrate stimulated with a 3.0-V electric field for 5 s. This meant that the hydrogel on foot B contacted an anode, thus generating high adhesion strength. Next, foot A took a step forward and attached to the substrate under the stimulation of a 3.0-V electric field for 5 s. Then, the electric field applied on foot B was switched into −3.0 V for 3 s, to make the hydrogel nonadhesive to the substrate. Thus, foot B detached from the substrate and took a step forward. After each electrical stimulation, the voltage applied on the robot feet was set to 0 V. In the case of locomotion on the inverted substrate (Fig. 4C and movie S8), robot no. 1 took its first step with foot A and climbed using the control program similar to that of vertical locomotion. By cycling this locomotion mode, robot no. 1 can climb on both near-vertical and inverted stainless steel surfaces, with average locomotion speeds of ~7.5 and ~7.8 cm/min, respectively.

A defect relating to robot no. 1 is the relatively large center of mass–to–substrate distance (~2.5 cm), which reduces its motion stability on vertical surfaces. Thus, we conservatively chose a substrate with an 85° inclination for the vertically climbing of robot no. 1. This issue is more obvious for robot no. 1 to climb on the copper surface, to which TBVA hydrogels have relatively low adhesion strength. Robot no. 1 often pitches back during climbing. Therefore, we designed another three-foot tethered walking robot (denoted as robot no. 2; weight, ~175 g; Fig. 5, A and B) with a smaller center of mass–to–substrate distance (~1.4 cm). Details for robot no. 2 can be found in Supplementary Text, table S4, and figs. S24 and S25. The sizes of hydrogels pasted on the feet of robot no. 2 were about 10.0 cm by 1.6 cm by 0.4 cm for foot A and 10.0 cm by 3.0 cm by 0.4 cm for foot B. Robot no. 2 adopts the same control program as robot no. 1. As expected, robot no. 2 can continuously climb on both a vertical (90°) stainless steel surface (Fig. 5C and movie S9) and a vertical copper surface (Fig. 5D and movie S10), with average moving speeds of ~8.1 and ~8.8 cm/min, respectively. Also, robot no. 2 can climb on an inverted copper surface (Fig. 5E and movie S11) at an average speed of ~8.7 cm/min.

We also designed a wheeled robot (denoted as robot no. 3; weight, ~180 g; Fig. 5, F and G; Supplementary Text; and figs. S26 and S27). Seven pieces of TBVA hydrogels with a size around 4.0 cm by 2.0 cm by 0.4 cm were assembled on each driving wheel of robot

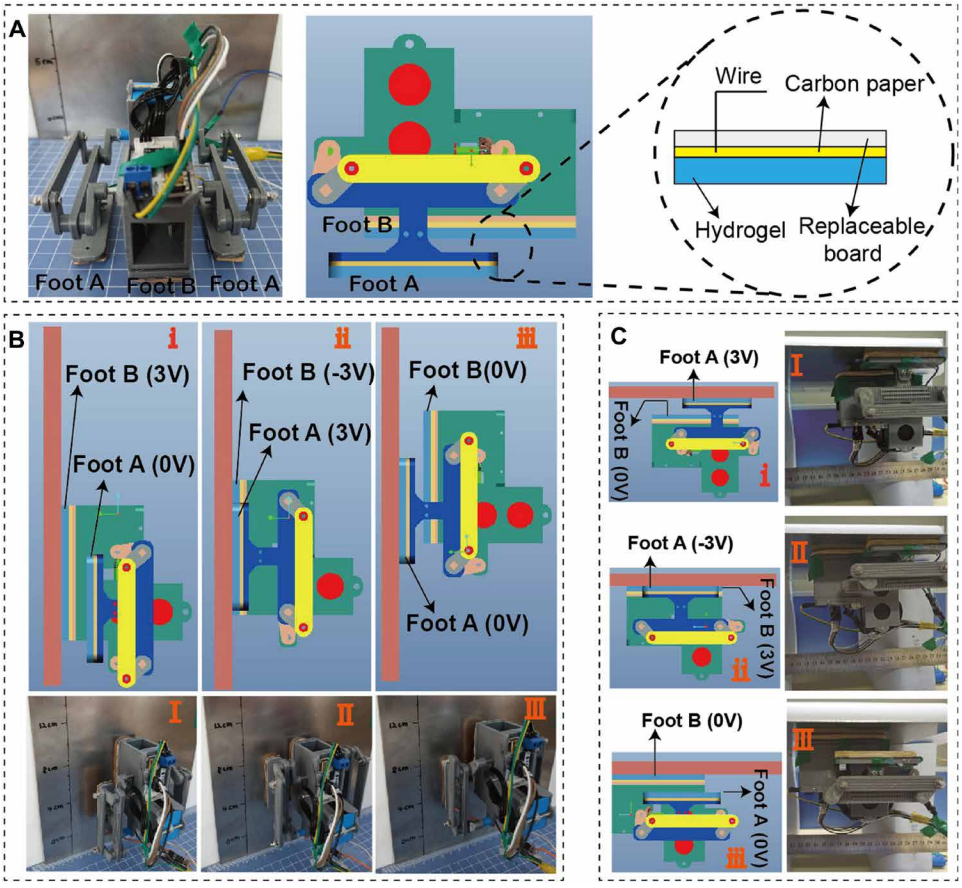

Fig. 4. Climbing performances of robot no. 1. (**A**) Photograph and structure of robot no. 1. Foot A and foot B are equipped with TBVA3 hydrogel. Electrical stimulation modes and photographs of robot no. 1 climbing on near-vertical (85°) (**B**) and inverted (**C**) stainless steel surfaces.

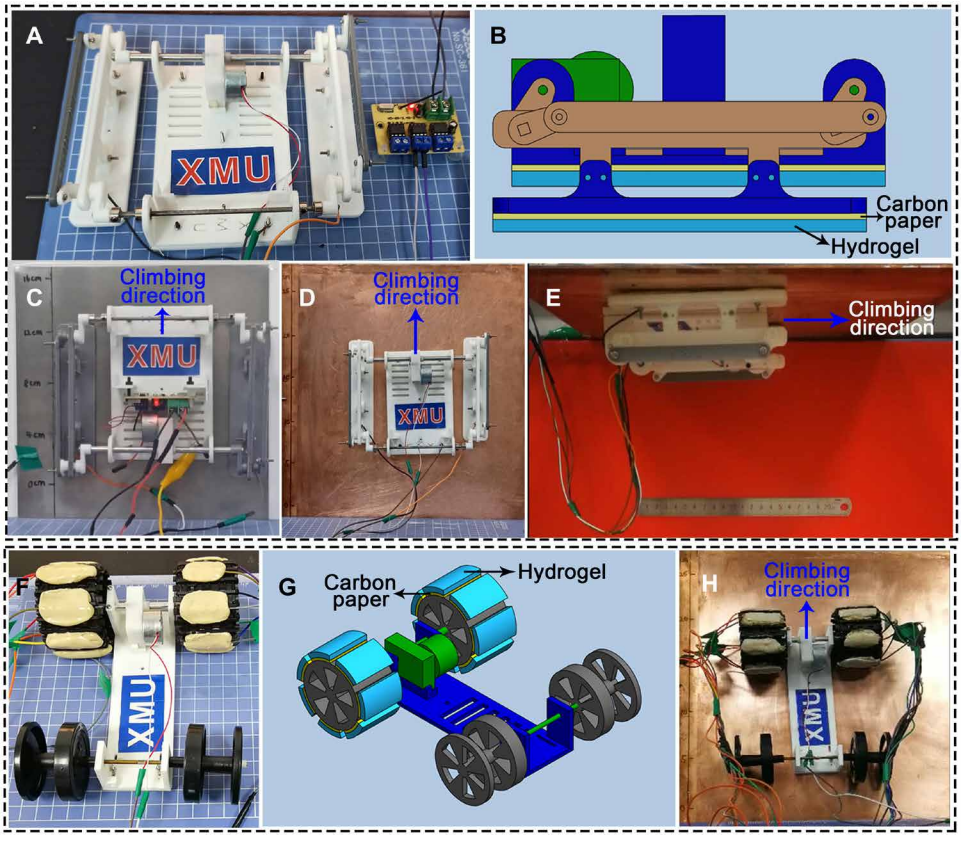

Fig. 5. Climbing performances of robot no. 2 and robot no. 3. Photograph (**A**) and structure (**B**) of robot no. 2. Photographs taken from the climbing of robot no. 2 on vertical (90°) stainless steel (**C**) and copper (**D**) surfaces, as well as on inverted copper surface (**E**). Photograph (**F**) and structure (**G**) of robot no. 3. A picture showing the climbing of robot no. 3 on near-vertical (85°) copper surface (**H**). The feet of robot no. 2 and the wheels of robot no. 3 are equipped with TBVA3 hydrogel.

no. 3. Carbon papers (thickness, 0.1 cm) were incorporated in the hydrogels to act as current collectors. The circuit of each piece of hydrogel was separately controlled. The control program of robot no. 3 is illustrated in fig. S28. Briefly, with the rotating of the driving wheels, when the first piece of hydrogel moved down to contact the substrate, its adhesiveness was activated by an electrical stimulus (3.0 V, 5 s). Then, the second piece of hydrogel moved down and attached to the substrate, under the stimulation of an electric field (3.0 V, 5 s). At the same time, the first piece of hydrogel detached from the substrate in response to a negative electric field (−3.0 V, 3 s). Each wheel kept one piece of hydrogel attaching to the substrate, and the corresponding voltage was set to 0 V after stimulation. By cycling this motion control mode, robot no. 3 can climb on near-vertical (85°) copper surface (Fig. 5H and movie S12) at an average speed of 13.5 cm/min. Theoretically, the contact area between the wheels and the substrate is limited because of the circular structure of the wheel. This reduces the attaching capability of wheeled robots to the vertical surface. Fortunately, the elasticity of TBVA hydrogels can improve the contacting area, thus ensuring the climbing of robot no. 3. However, strong shear force also occurs to the hydrogel during the robot climbing and causes hydrogel deformation. This is an important reason why we choose a near-vertical substrate for the climbing of the wheeled robot. In general, by using three simple prototypical robots, we demonstrated the possibility of using polymeric adhesives as the robots' moving parts to climb on both vertical and inverted surfaces.

DISCUSSION

We have developed a facile and scalable strategy to fabricate borate ester polymer hydrogels to serve as programmable adhesives for climbing robots. Under the stimulation of a mild electric field, this hydrogel can rapidly and reversibly switch between adhesive and nonadhesive states. By simply pasting this hydrogel on the moving parts of robots, we have realized the climbing of both walking robots and wheeled robots on different surfaces. Our study shows that the challenges in robot climbing, such as complicated material microstructure and device designs, and the technical threshold for high-level engineering (*3*, *54*), may be potentially overcome through a polymer network regulation approach. Programming the adhesive/nonadhesive evolution based on the concept of adhesive promoter exposing/shielding may provide an avenue for engineering adhesive materials. In addition to the electrical sensitivity, this hydrogel also demonstrates promising mechanical strength, easy processability, and rapid self-healing performance, making it potentially useful in the fields of electronic skin (*55*), wearable device (*56*), tissue adhesion (*57*), sensing (*58*), flexible energy storage device (*59*), and so on.

At present, our stimuli-responsive adhesive hydrogels only provide a conceptual route for the design of climbing robots. Both the adhesion strength of the hydrogels and the climbing speed of the robots failed to surpass other well-developed climbing technologies. However, our hydrogel has the potential to be broadly applied to variety of robot designs because it has no specific requirements for the device structure, power supply, and even locomotion mode.

Rational designs of the hydrogel composition and structure may potentially enhance the adhesion strength. For example, we have improved the mechanical and adhesive properties of the hydrogels through a simple cross-linker structure adjustment (fig. S29). Also, the climbing robots can be designed with an increased compatibility with the hydrogels, therefore increasing the climbing speed.

Future research will try to overcome the limitations derived from the adhesion evolution mechanism, and the intrinsic physical and mechanical properties of the hydrogels. The first issue is that our hydrogels seem to have programmable adhesion only on conductive surfaces. Researchers have verified the excellent adhesive performance of catechol functionalized polymers on nonconductive surfaces (*35*, *60*, *61*). Therefore, the key point for our hydrogels to work on nonconductive surfaces is to ensure the electrically triggered exposure of catechol groups. We have found that this may be

achieved by embedding an electrode (such as stainless steel mesh) on the hydrogel surface (fig. S30A). The electrode ensures the effective water electrolysis reaction, whereas the hydrogel bulging from the meshes enables good contacts with the nonconductive surface. With this design, the attaching/detaching behavior of TBVA hydrogels also occurs on the nonconductive glass (adhesion strength, ~9.5 kPa; fig. S30, B and C). This is part of our ongoing work to realize robot climbing on nonconductive surfaces.

The second issue relates to the dehydration of the hydrogels. For example, at room temperature and atmospheric pressure, TBVA3 exhibits ~21.2 and 31.3 wt % of dehydrations after 24 and 48 hours (fig. S31A), respectively. However, TBVA3 shows enhanced mechanical strength after dehydration because of the reduced water content (fig. S31B). The adhesive and electrically responsive properties of TBVA3 maintain well within ~21.2 wt % of dehydration, because 5 s of electrical stimulation (3.0 V) generates adhesion strength ≥11.0 kPa on stainless steel (fig. S31C), which is comparable to newly prepared TBVA3. Detailed results are given in the Supplementary Materials. For potentially practical applications, 24 hours may be enough for a climbing robot to finish one task. Moreover, TBVA hydrogels are prepared from a straightforward synthetic procedure, and they are simply pasted on the climbing robots. It is possible to alternate the TBVA hydrogels once they lose efficacy. Our ongoing research includes the design of hydrogel composition and microphase, thus reducing the dehydration speed.

In addition, climbing robots that can work in an underwater environment are of great practical value. Although many catechol-functionalized polymers show adhesion to wet surfaces (*32*, *33*, *60*), it remains a challenge to achieve underwater reversible attachment/detachment. To realize the use of our hydrogels in an underwater environment, it is important to integrate an electrode on the hydrogel surface (fig. S30), thus potentially addressing the problem of short circuit during electrical stimulation. The borate ester should be replaced by boronate esters that can be stably bonded onto the polymer chains, and the conductive ions need to be covalently attached onto the polymer networks. These designs may be effective in avoiding the leakage of cross-linker and ions from the hydrogels into water. Also, the pH and ionic strength of the water should be fully considered when applying the hydrogels in an underwater environment. Future research will also seek effective ways to extend this electrically switchable adhesion mechanism to non–water-containing adhesive materials.

MATERIALS AND METHODS

Materials

PVA (DP, 1700; Mw, ~79,000 g/mol; alcoholysis, 99.8 to 100%), BA, and KOH were purchased from Aladdin. TTS was supplied by J&K Chemical. These chemicals were used as received without further purification. Substrates (stainless steel, carbon paper, ITO, Al, Cu, and nonconductive glass) for the adhesion tests or robot climbing experiments were purchased from J&K Chemical. These substrates were thoroughly cleaned by sonication in ethanol and deionized water, followed by vacuum drying (60°C) overnight.

Hydrogel synthesis

Preparation of cross-linker TB

TTS (0.8 g, 2.35 mmol), BA (0.154 g, 2.50 mmol), and KOH (0.14 g, 2.50 mmol) were introduced into 7 ml of deionized water. After stirring at 90°C for 2 hours, the reaction mixture was cooled to room temperature and filtrated to remove unreacted TTS. TB powder was obtained after a freeze-drying procedure.

Preparation of TBVA hydrogels

TB was dissolved in water and introduced into a water solution of PVA (0.2 g/ml). The pH of the reaction system was controlled at ~8.5 by using KOH aqueous solution. The mixture was vigorously stirred for 1 hour at 90°C and then cooled to room temperature. After an additional 24 hours of aging procedure, TBVA hydrogels were prepared. The water content of the hydrogels was fixed at ~85 wt %, whereas the cross-linking density of the hydrogels was controlled by tuning the content of TB. As a control experiment, we also fabricated BVA hydrogel by directly cross-linking PVA with BA using the same procedure. The content of BA in BVA hydrogel was fixed at 4.0 wt %.

Characterization

FTIR spectra were characterized on a Nicolet Avatar 360. ^{1}H NMR spectra were acquired on a Bruker Avance 400-MHz spectrometer. XPS measurement of the freeze-dried hydrogel was conducted on a PHI Quantum-2000 electron spectrometer. Water contact angles on the surfaces of the hydrogels molded with different substrates were measured on an optical contact angle meter (DSA20, KRüSS). Substrates including hydrophilic glass, ceramic, poly(methylmethacrylate), copper, PTFE, and hydrophobic glass were adopted to mold the hydrogels. All tests were repeated at least five times. Microscopic image analysis system (MF600D-TFBD) was adopted to track the crack recovery on the surfaces of TBVA hydrogels and probe the surfaces of the substrates after hydrogel attachment/detachment. The healing time was statistically calculated from five parallel experiments. Scanning electron microscopy (SEM) images and energy-dispersive spectrometer mappings were taken from a HiTaChi SU-70 SEM instrument.

The mechanical properties of the hydrogels were measured on a universal testing machine (AGS-X). The stretching speed was fixed at 10 cm/min. Hydrogels were molded into a size of 3.0 cm by 1.0 cm by 0.4 cm. The rheological behavior of the hydrogels was characterized on a rheometer (Anton Paar, MCR 302) using a flat plate mode (the diameter of the upper plate was 2.5 cm and the selected gap was 0.1 cm). The samples were sealed with silicone oil to reduce water loss. The strain (γ) sweep test was conducted at γ ranging from 0.01 to 100%, frequency (f) of 2π rad/s (1 Hz), and temperature (T) of 25°C. The frequency (ω) sweep test was conducted at ω ranging from 0.1 to 100 rad/s, γ of 0.5%, and T of 25°C. The temperature (T) sweep test was conducted at T ranging from 25° to 80°C, γ of 0.5%, and f of 2π rad/s (1 Hz).

For the self-healing characterization, the hydrogels (3.0 cm by 1.0 cm by 0.4 cm) were cut into two pieces. The two hydrogel pieces were connected at room temperature. After healing for a certain time, the tensile test was conducted (stretching speed, 10 cm/min). Each test was repeated five times by using different samples. To gain an insight into the self-healing properties of TBVA hydrogels, a programmed rheological measurement was adopted. Strain (γ) and duration were set as follows: 0.5% (120 s) → 80% (60 s) → 0.5% (120 s) → 80% (60 s) → 0.5% (120 s) → 80% (60 s). The time dependences of G' and G'' were recorded during step strain measurements at ω = 2π rad/s (1 Hz) and 25°C. Small strain (0.5%) was set for recovering after inner structure breaking of the hydrogels, and large strain (80%) was set for breaking the inner structure according to

the strain sweep. Time for healing was set to 120 s because the self-healing efficiency reached ~100% in such a time scale, according to the tensile test results. Time for breaking was set to 60 s.

Electrochemical test

The electrochemical measurements were performed on an electrochemical workstation (CHI 760E). CV curves of TTS and TB were acquired using a typical three-electrode system. Glassy carbon or stainless steel was adopted as the working electrode. Pt foil and Hg/HgO (1.0 M KOH) were used as counter electrode and reference electrode, respectively. Aqueous electrolytes applied in this measurement comprised 0.1 mmol/ml of TTS or TB. The pH of these electrolytes was adjusted to ~8.5 using KOH. The CV curves of TBVA hydrogels were characterized by sandwiching the hydrogel samples (thickness, 0.12 cm) between two stainless steel electrodes.

The electrochemical impedance spectroscopy (EIS) test was conducted on Autolab PGSTAT 302N. Hydrogel samples were shaped into a size of 1.2 cm by 1.0 cm by 0.12 cm and sandwiched between two stainless steel electrodes. EIS spectra were recorded with frequency ranging from 0.1 to 10^6 Hz (voltage amplitude, 5 mV). Each test was repeated at least five times. The bulk resistances of the hydrogels were determined from the intercepts of the semicircle with the real axis in the Nyquist plots. The conductivity was eventually calculated using the following equation

$$\sigma = \frac{L \times 1000}{R \times S}$$

where L is the hydrogel thickness (unit, centimeter), S is the electrode surface area (unit, square centimeter), and R is the bulk membrane resistance (unit, ohm).

Adhesion test

The device for the adhesion test is illustrated in Fig. 3B. Hydrogel samples were molded into a size of 3.0 cm by 1.0 cm by 0.4 cm. One end of the hydrogel was connected to the substrates (stainless steel, carbon paper, ITO, Al, Cu, and nonconductive glass); the other end was fixed to a clamp with a stainless steel mesh as the electrode. The substrate and electrode were connected to a DC power. The distance (d) between the stainless steel mesh (lower edge) and the substrate was set to 1.5 or 2.0 cm. This device was fixed on the universal testing machine. Tensile stress-strain curves of TBVA hydrogels after electrical stimulation were characterized. All measurements were repeated at least five times.

Locomotion of climbing robots

Robots no. 1 and no. 2 are three-foot tethered climbing robots, and robot no. 3 is a wheeled tethered climbing robot. The weights of these robots do not include circuit board, wiring, and battery. The climbing performances of these robots were tested on near-vertical (85°), completely vertical (90°), and inverted surfaces. TBVA3 was pasted on the feet or wheels of the robots. The attachment/detachment switch was controlled by the electric field direction. Substrates including stainless steel and copper were adopted. The design, parameters, and logical control of the robots are described in the Supplementary Materials.

SUPPLEMENTARY MATERIALS

robotics.sciencemag.org/cgi/content/full/6/52/eabe1858/DC1
Supplementary Text
Fig. S1. FTIR spectra of the hydrogel cross-linker.
Fig. S2. ^{1}H NMR spectra.
Fig. S3. Hydrogel composition analyses.
Fig. S4. Hydrogel surface properties.
Fig. S5. Mechanical property evolution versus hydrogel water content.
Fig. S6. Hydrogel rheology properties.
Fig. S7. Control experiments for self-healing performance.
Fig. S8. Hydrogel conductivity.
Fig. S9. Hydrogel adhesion performance variation versus stimulation voltage.
Fig. S10. Adhesion performance of the hydrogel with an enlarged sample length.
Fig. S11. Effect of water content on the hydrogel electrical response.
Fig. S12. Electrochemical characteristics of the hydrogel cross-linker.
Fig. S13. Electrochemical characteristics of the hydrogel.
Fig. S14. The method for hydrogel surface pH control.
Fig. S15. Effect of surface pH on the hydrogel adhesiveness.
Fig. S16. Electrically induced hydrogel surface composition variation.
Fig. S17. Electrodeposition of the cross-linker solution.
Fig. S18. Morphology and composition evolutions of the substrate surfaces after hydrogel attachment/detachment.
Fig. S19. Electrically triggered attachment of the hydrogel to different substrates.
Fig. S20. Hydrogel self-healing during attaching/detaching process.
Fig. S21. The structure of robot no. 1.
Fig. S22. Three-view of robot no. 1.
Fig. S23. The whole circuit for robot no. 1.
Fig. S24. The structure of robot no. 2.
Fig. S25. Three-view of robot no. 2.
Fig. S26. The structure of robot no. 3.
Fig. S27. Three-view of robot no. 3.
Fig. S28. The electrical stimulation mode for robot no. 3 climbing.
Fig. S29. Molecular structure extension of the hydrogel design.
Fig. S30. Attaching/detaching performance of the hydrogel on nonconductive glass.
Fig. S31. Mechanical and adhesion performances of the dehydrated hydrogels.
Table S1. Characteristic peaks of FTIR spectra.
Table S2. Summary of hydrogel mechanical performances.
Table S3. Parameters of servo for robot no. 1.
Table S4. Parameters of reduction motor for robot no. 2.
Movie S1. Self-healing experiment.
Movie S2. Adhesion generation to carry 100 g of weight.
Movie S3. Adhesion generation on stainless steel.
Movie S4. Adhesion measurement on a tensile machine.
Movie S5. Reversible attachment/detachment on stainless steel.
Movie S6. Electrolysis of water in a TB solution.
Movie S7. Robot no. 1 climbing on near-vertical (85°) stainless steel surface.
Movie S8. Robot no. 1 climbing on inverted stainless steel surface.
Movie S9. Robot no. 2 climbing on vertical (90°) stainless steel surface.
Movie S10. Robot no. 2 climbing on vertical (90°) copper surface.
Movie S11. Robot no. 2 climbing on inverted copper surface.
Movie S12. Robot no. 3 climbing on near-vertical (85°) copper surface.
References (*62*, *63*)

REFERENCES AND NOTES

1. G. Gu, J. Zou, R. Zhao, X. Zhao, X. Zhu, Soft wall-climbing robots. *Sci. Robot.* **3**, eaat2874 (2018).
2. A. Nishi, Development of wall-climbing robots. *Comput. Electr. Eng.* **22**, 123–149 (1996).
3. M. K. Kwak, C. Pang, H.-E. Jeong, H.-N. Kim, H. Yoon, H.-S. Jung, K.-Y. Suh, Towards the next level of bioinspired dry adhesives: New designs and applications. *Adv. Funct. Mater.* **21**, 3606–3616 (2011).
4. J. Purtov, M. Frensemeier, E. Kroner, Switchable adhesion in vacuum using bio-inspired dry adhesives. *ACS Appl. Mater. Interfaces* **7**, 24127–24135 (2015).
5. A. K. Geim, S. V. Dubonos, I. V. Grigorieva, K. S. Novoselov, A. A. Zhukov, S. Y. Shapoval, Microfabricated adhesive mimicking gecko foot-hair. *Nat. Mater.* **2**, 461–463 (2003).
6. D. Tao, X. Gao, H. Lu, Z. Liu, Y. Li, H. Tong, N. Pesika, Y. Meng, Y. Tian, Controllable anisotropic dry adhesion in vacuum: Gecko inspired wedged surface fabricated with ultraprecision diamond cutting. *Adv. Funct. Mater.* **27**, 1606576 (2017).
7. D. Ruffatoo III, A. Parness, M. Spenko, Improving controllable adhesion on both rough and smooth surfaces with a hybrid electrostatic/gecko-like adhesive. *J. R. Soc. Interface* **11**, 20131089 (2014).
8. S. Song, D.-M. Drotlef, C. Majidi, M. Sitti, Controllable load sharing for soft adhesive interfaces on three-dimensional surfaces. *Proc. Natl. Acad. Sci. U.S.A.* **114**, E4344–E4353 (2017).
9. M. T. Northen, C. Greiner, E. Arzt, K. L. Turner, A gecko-inspired reversible adhesive. *Adv. Mater.* **20**, 3905–3909 (2008).

10. Y. Ma, S. Ma, Y. Wu, X. Pei, S. N. Gorb, Z. Wang, W. Liu, F. Zhou, Remote control over underwater dynamic attachment/detachment and locomotion. *Adv. Mater.* **30**, 1801595 (2018).
11. H. Jiang, E. W. Hawkes, C. Fuller, M. A. Estrada, S. A. Suresh, N. Abcouwer, A. K. Han, S. Wang, C. J. Ploch, A. Parness, M. R. Cutkosky, A robotic device using gecko-inspired adhesives can grasp and manipulate large objects in microgravity. *Sci. Robot.* **2**, eaan4545 (2017).
12. M. A. Graule, P. Chirarattananon, S. B. Fuller, N. T. Jafferis, K. Y. Ma, M. Spenko, R. Kornbluh, R. J. Wood, Perching and takeoff of a robotic insect on overhangs using switchable electrostatic adhesion. *Science* **352**, 978–982 (2016).
13. M. Tavakoli, C. Viegas, L. Marques, J. N. Pires, A. T. De Almeida, OmniClimbers: Omni-directional magnetic wheeled climbing robots for inspection of ferromagnetic structures. *Robot. Auton. Syst.* **61**, 997–1007 (2013).
14. M. Fujita, S. Lkeda, T. Fujimoto, T. Shimizu, S. Ikemoto, T. Miyamoto, Development of universal vacuum gripper for wall-climbing robot. *Adv. Robot.* **32**, 283–296 (2018).
15. C. Wang, J. Wu, G. M. Bernard, Preparation and characterization of canola protein isolate-poly (glycidyl methacrylate) conjugates: A bio-based adhesive. *Ind. Crop. Prod.* **57**, 124–131 (2014).
16. B. P. Lee, P. B. Messersmith, J. N. Israelachvili, J. H. Waite, Mussel-inspired adhesives and coatings. *Annu. Rev. Mater. Res.* **41**, 99–132 (2011).
17. X. Ji, M. Ahmed, L. Long, N. M. Khashab, F. Huang, J. L. Sessler, Adhesive supramolecular polymeric materials constructed from macrocycle-based host-guest interactions. *Chem. Soc. Rev.* **48**, 2682–2697 (2019).
18. J. Luo, J. Luo, Y. Bai, Q. Gao, J. Li, A high performance soy protein-based bio-adhesive enhanced with a melamine/epichlorohydrin prepolymer and its application on plywood. *RSC Adv.* **6**, 67669–67676 (2016).
19. J. W. Seo, H. Kim, K. Kim, S. Q. Choi, H. J. Lee, Calcium-modified silk as a biocompatible and strong adhesive for epidermal electronics. *Adv. Funct. Mater.* **28**, 1800802 (2018).
20. V. Granskog, S. Garcia-Gallego, J. von Kieseritzky, J. Rosendahl, P. Stenlund, Y. Zhang, S. Petronis, B. Lyvén, M. Arner, J. Håkansson, M. Malkoch, High-performance thiol-ene composites unveil a new era of adhesives suited for bone repair. *Adv. Funct. Mater.* **28**, 1800372 (2018).
21. M. A. Gonzalez, J. R. Simon, A. Ghoorchian, Z. Scholl, S. Lin, M. Rubinstein, P. Marszalek, A. Chilkoti, G. P. López, X. Zhao, Strong, tough, stretchable, and self-adhesive hydrogels from intrinsically unstructured proteins. *Adv. Mater.* **29**, 1604743 (2017).
22. X. Zhang, M. Wang, T. Jia, X. Ma, Q. Song, Q. Zhou, X. Yang, J. Liu, A. Guo, A heat-resistant glass-modified multi-component phosphate adhesive for repair and connection of superalloy in extreme environment. *J. Alloys Compd.* **745**, 868–873 (2018).
23. M. Wang, X. Tao, X. Xu, R. Miao, H. Du, J. Liu, A. Guo, High-temperature bonding performance of modified heat-resistant adhesive for ceramic connection. *J. Alloys Compd.* **663**, 82–85 (2016).
24. A. H. Hofman, I. A. van Hees, J. Yang, M. Kamperman, Bioinspired underwater adhesives by using the supramolecular toolbox. *Adv. Mater.* **30**, 1704640 (2018).
25. H. Shao, R. J. Stewart, Biomimetic underwater adhesives with environmentally triggered setting mechanisms. *Adv. Mater.* **22**, 729–733 (2010).
26. A. R. Narkar, B. Barker, M. Clisch, J. Jiang, B. P. Lee, pH responsive and oxidation resistant wet adhesive based on reversible catechol-boronate complexation. *Chem. Mater.* **28**, 5432–5439 (2016).
27. A. R. Narkar, B. P. Lee, Incorporation of anionic monomer to tune the reversible catechol-boronate complex for pH-responsive, reversible adhesion. *Langmuir* **34**, 9410–9417 (2018).
28. C. Creton, Pressure-sensitive adhesives: An introductory course. *MRS Bull.* **28**, 434–439 (2003).
29. H. Yi, M. Seong, K. Sun, I. Hwang, K. Lee, C. Cha, T. Kim, H. E. Jeong, Wet-responsive, reconfigurable, and biocompatible hydrogel adhesive films for transfer printing of nanomembranes. *Adv. Funct. Mater.* **28**, 1706498 (2018).
30. Y. Zhao, Y. Wu, L. Wang, M. Zhang, X. Chen, M. Liu, J. Fan, J. Liu, F. Zhou, Z. Wang, Bio-inspired reversible underwater adhesive. *Nat. Commun.* **8**, 2218 (2017).
31. A. C. Ferahian, D. K. Hohl, C. Weder, L. Montero de Espinosa, Bonding and debonding on demand with temperature and light responsive supramolecular polymers. *Macromol. Mater. Eng.* **304**, 1900161 (2019).
32. P. K. Forooshani, B. P. Lee, Recent approaches in designing bioadhesive materials inspired by mussel adhesive protein. *J. Polym. Sci. A Polym. Chem.* **55**, 9–33 (2017).
33. J. Saiz-Poseu, J. Mancebo-Aracil, F. Nador, F. Busqué, D. Ruiz-Molina, The chemistry behind catechol-based adhesion. *Angew. Chem. Int. Ed.* **58**, 696–714 (2019).
34. Q. Ye, F. Zhou, W. Liu, Bioinspired catecholic chemistry for surface modification. *Chem. Soc. Rev.* **40**, 4244–4258 (2011).
35. M. Liao, P. Wan, J. Wen, M. Gong, X. Wu, Y. Wang, R. Shi, L. Zhang, Wearable, healable, and adhesive epidermal sensors assembled from mussel-inspired conductive hybrid hydrogel framework. *Adv. Funct. Mater.* **27**, 1703852 (2017).
36. W. Tang, G. M. Policastro, G. Hua, K. Guo, J. Zhou, C. Wesdemiotis, G. L. Doll, M. L. Becker, Bioactive surface modification of metal oxides via catechol-bearing modular peptides: Multivalent-binding, surface retention, and peptide bioactivity. *J. Am. Chem. Soc.* **136**, 16357–16367 (2014).
37. M.-H. Ryou, J. Kim, I. Lee, S. Kim, Y. K. Jeong, S. Hong, J. H. Ryu, T.-S. Kim, J.-K. Park, H. Lee, J. W. Choi, Mussel-inspired adhesive binders for high-performance silicon nanoparticle anodes in lithium-ion batteries. *Adv. Mater.* **25**, 1571–1576 (2013).
38. P. Wilke, N. Helfricht, A. Mark, G. Papastavrou, D. Faivre, H. G. Börner, A direct biocombinatorial strategy toward next generation, mussel-glue inspired saltwater adhesives. *J. Am. Chem. Soc.* **136**, 12667–12674 (2014).
39. Y. Li, L. Yang, Y. Zeng, Y. Wu, Y. Wei, L. Tao, Self-healing hydrogel with a double dynamic network comprising imine and borate ester linkages. *Chem. Mater.* **31**, 5576–5583 (2019).
40. J. H. Woo, N. H. Kim, S. I. Kim, O.-K. Park, J. H. Lee, Effects of the addition of boric acid on the physical properties of MXene/polyvinyl alcohol (PVA) nanocomposite. *Compos. Part B* **199**, 108205 (2020).
41. D. Li, Y. Chen, Z. Liu, Boronate affinity materials for separation and molecular recognition: Structure, properties and applications. *Chem. Soc. Rev.* **44**, 8097–8123 (2015).
42. G. Yang, J. Zhao, L. Cui, S. Song, S. Zhang, L. Yu, P. Zhang, Tribological characteristic and mechanism analysis of borate ester as a lubricant additive in different base oils. *RSC Adv.* **7**, 7944–7953 (2017).
43. S. Huang, S. Su, H. Gan, L. Wu, C. Lin, D. Xu, H. Zhou, X. Lin, Y. Qin, Facile fabrication and characterization of highly stretchable lignin-based hydroxyethyl cellulose self-healing hydrogel. *Carbohydr. Polym.* **223**, 115080 (2019).
44. J. Liu, J. Huang, Q. Cai, Y. Yang, W. Luo, B. Zeng, Y. Xu, C. Yuan, L. Dai, Design of slidable polymer networks: A rational strategy to stretchable, rapid self-healing hydrogel electrolytes for flexible supercapacitors. *ACS Appl. Mater. Interfaces* **12**, 20479–20489 (2020).
45. W.-P. Chen, D.-Z. Hao, W.-J. Hao, X.-L. Guo, L. Jiang, Hydrogel with ultrafast self-healing property both in air and underwater. *ACS Appl. Mater. Interfaces* **10**, 1258–1265 (2018).
46. C. C. Deng, W. L. Brooks, K. A. Abboud, B. S. Sumerlin, Boronic acid-based hydrogels undergo self-healing at neutral and acidic pH. *ACS Macro Lett.* **4**, 220–224 (2015).
47. Z. Wang, Y. Cong, J. Fu, Stretchable and tough conductive hydrogels for flexible pressure and strain sensors. *J. Mater. Chem. B* **8**, 3437–3459 (2020).
48. D. Li, G. Zhou, S. Gu, T. Zhang, L. Meng, Y. Guo, T. Deng, Thermodynamic and dynamic modeling of the boron species in aqueous potassium borate solution. *ACS Omega* **5**, 15835–15842 (2020).
49. M. Şenel, A. Bozkurt, A. Baykal, An investigation of the proton conductivities of hydrated poly(vinyl alcohol)/boric acid complex electrolytes. *Ionics* **13**, 263–266 (2007).
50. M. J. Garland, T. R. R. Singh, A. D. Woolfson, R. F. Donnelly, Electrically enhanced solute permeation across poly(ethylene glycol)-crosslinked poly(methyl vinyl ether-co-maleic acid) hydrogels: Effect of hydrogel crosslink density and ionic conductivity. *Int. J. Pharm.* **406**, 91–98 (2011).
51. M. E. Smithmyer, C. C. Deng, S. E. Cassel, P. J. LeValley, B. S. Sumerlin, A. M. Kloxin, Self-healing boronic acid-based hydrogels for 3D co-cultures. *ACS Macro Lett.* **7**, 1105–1110 (2018).
52. Y. Chen, W. Qian, R. Chen, H. Zhang, X. Li, D. Shi, W. Dong, M. Chen, Y. Zhao, One-pot preparation of autonomously self-healable elastomeric hydrogel from boric acid and random copolymer bearing hydroxyl groups. *ACS Macro Lett.* **6**, 1129–1133 (2017).
53. M. S. A. Bhuiyan, J. D. Roland, B. Liu, M. Reaume, Z. Zhang, J. D. Kelley, B. P. Lee, In situ deactivation of catechol-containing adhesive using electrochemistry. *J. Am. Chem. Soc.* **142**, 4631–4638 (2020).
54. T. Seo, Y. Jeon, C. Park, J. Kim, Survey on glass and façade-cleaning robots: Climbing mechanisms, cleaning methods, and applications. *Int. J. Pr. Eng. Man.-G.T.* **6**, 367–376 (2019).
55. B. Ryplida, K. D. Lee, I. In, S. Y. Park, Light-induced swelling-responsive conductive, adhesive, and stretchable wireless film hydrogel as electronic artificial skin. *Adv. Funct. Mater.* **29**, 1903209 (2019).
56. P. Li, Z. Jin, L. Peng, F. Zhao, D. Xiao, Y. Jin, G. Yu, Stretchable all-gel-state fiber-shaped supercapacitors enabled by macromolecularly interconnected 3D graphene/nanostructured conductive polymer hydrogels. *Adv. Mater.* **30**, 1800124 (2018).
57. L. Han, K. Liu, M. Wang, K. Wang, L. Fang, H. Chen, J. Zhou, X. Lu, Mussel-inspired adhesive and conductive hydrogel with long-lasting moisture and extreme temperature tolerance. *Adv. Funct. Mater.* **28**, 1704195 (2018).
58. M. Qin, M. Sun, R. Bai, Y. Mao, X. Qian, D. Sikka, Y. Zhao, H. J. Qi, Z. Suo, X. He, Bioinspired hydrogel interferometer for adaptive coloration and chemical sensing. *Adv. Mater.* **30**, 1800468 (2018).
59. Z. Liu, G. Liang, Y. Zhan, H. Li, Z. Wang, L. Ma, Y. Wang, X. Niu, C. Zhi, A soft yet device-level dynamically super-tough supercapacitor enabled by an energy-dissipative dual-crosslinked hydrogel electrolyte. *Nano Energy* **58**, 732–742 (2019).

60. P. Glass, H. Chung, N. R. Washburn, M. Sitti, Enhanced reversible adhesion of dopamine methacrylamide-coated elastomer microfibrillar structures under wet conditions. *Langmuir* **25**, 6607–6612 (2009).
61. B. J. Sparks, E. F. T. Hoff, L. P. Hayes, D. L. Patton, Mussel-inspired thiol-ene polymer networks: Influencing network properties and adhesion with catechol functionality. *Chem. Mater.* **24**, 3633–3642 (2012).
62. M. Lu, S. Huang, S. Chen, Q. Ju, M. Xiao, X. Peng, S. Wang, Y. Meng, Transparent and super-gas-barrier PET film with surface coated by a polyelectrolyte and borax. *Polym. J.* **50**, 239–250 (2018).
63. J.-Y. Sun, X. Zhao, W. R. K. Illeperuma, O. Chaudhuri, K. H. Oh, D. J. Mooney, J. J. Vlassak, Z. Suo, Highly stretchable and tough hydrogels. *Nature* **489**, 133–136 (2012).

Acknowledgments: We thank C.-J. Zhong of the State University of New York at Binghamton for the help with the language checking of the manuscript. **Funding:** This work was supported by the National Natural Science Foundation of China (52033008, 51773172, and 51673161); the Natural Science Foundation of Fujian Province of China (2020J06005). **Author contributions:** C.Y. and L.D. conceived the project. J.H. conducted the hydrogel synthesis and characterization and the robot climbing experiments. Y.L. and Z.Z. designed and assembled the climbing robots. Y.Y., J.M., T.W., J.L., Q.C., and C.P. carried out the mechanical and adhesion measurements of the hydrogels. Y.X., B.Z., W.L., and G.C. analyzed the data. C.Y., J.H., and L.D. wrote the manuscript. **Competing interests:** The authors declare that they have no competing interests. **Data and materials availability:** All data are available in the main text or the Supplementary Materials.

Submitted 5 August 2020
Accepted 17 March 2021
Published 14 April 2021
10.1126/scirobotics.abe1858

Citation: J. Huang, Y. Liu, Y. Yang, Z. Zhou, J. Mao, T. Wu, J. Liu, Q. Cai, C. Peng, Y. Xu, B. Zeng, W. Luo, G. Chen, C. Yuan, L. Dai, Electrically programmable adhesive hydrogels for climbing robots. *Sci. Robot.* **6**, eabe1858 (2021).

Science Robotics

Electrically programmable adhesive hydrogels for climbing robots

Junwen Huang, Yu Liu, Yuxin Yang, Zhijun Zhou, Jie Mao, Tong Wu, Jun Liu, Qipeng Cai, Chaohua Peng, Yiting Xu, Birong Zeng, Weiang Luo, Guorong Chen, Conghui Yuan, and Lizong Dai

Sci. Robot. **6** (53), eabe1858. DOI: 10.1126/scirobotics.abe1858

Science Robotics (ISSN 2470-9476) is published by the American Association for the Advancement of Science. 1200 New York Avenue NW, Washington, DC 20005. The title *Science Robotics* is a registered trademark of AAAS.